Available online at www.sciencedirect.com
ScienceDirect
Journal of Power Sources 161 (2006) 40–46
JOURNAL OF POWER SOURCES
www.elsevier.com/locate/jpowsour

Proton conduction in ceria-doped $Ba_2In_2O_5$ nanocrystalline ceramic at low temperature

Rob Hui [a,*], Radenka Maric [a], Cyrille Decès-Petit [a], Edward Styles [a], Wei Qu [a], Xinge Zhang [a], Justin Roller [a], Sing Yick [a], Dave Ghosh [a], Ko Sakata [b], Murata Kenji [b]

[a] *NRC-Institute for Fuel Cell Innovation, SOFC Group, 3250 East Mall, Vancouver, BC, Canada V6T 1W5*
[b] *The Institute of Applied Energy, Tokyo, Japan*

Received 20 February 2006; received in revised form 15 March 2006; accepted 28 March 2006
Available online 8 May 2006

Abstract

Sintered pellets of Ce-doped $Ba_2In_2O_5$ (BIC) were prepared from nanopowders. The electrical conductivities were measured using ac impedance spectroscopy under different atmospheres and temperatures. The electrical conductivity of sintered BIC was found sensitive to environmental humidity when the temperature was below 300 °C. However, in the presence of hydrogen, the electrical conductivities were independent of water content in the range of 0–30 vol%. The electrical conductivities of BIC were significantly affected by the presence of hydrogen in a temperature range of 100–300 °C. The estimated protonic transference number and the measured open circuit voltage suggested the existence of electronic conduction. The coefficient of thermal expansion of BIC is $11.2 \times 10^{-6}\ K^{-1}$ from 25 to 1250 °C.

Keywords: Proton conductor; Ceramics; Nanocrystalline; Low temperature; $Ba_2In_2O_5$

1. Introduction

Fuel cell technology has enormous promise for efficient and environmentally friendly mobile and stationary power applications. To enable widespread commercialization, higher performance with liquid fuels is needed. A paradigm shift in materials is required to achieve this. One of the enabling technologies is proton-conducting ceramic that can operate at temperatures above 100 °C to enable the more efficient use of reformate and hydrocarbon fuels. The vast majority of PEM fuel cells under commercial development use Nafion® as the proton conductor operating well below 100 °C. With strongly acidic $–SO_3H$ groups terminated as side chains, Nafion® requires substantial amounts of liquid water to maintain its high proton conductivity. Although PEM fuel cells based on Nafion® electrolytes are presently one of the most successful fuel cells developed, water distribution and transport within PEM fuel cells must be managed so as to continuously generate electric power. Since their conductivity is highly dependent on water content, a sudden drop is observed as the temperature approaches 100 °C. Methanol crossover in direct methanol fuel cells is strongly associated with the presence of water. Moreover, its high cost is still prohibitive for wide commercial applications. On the other hand, the absence of liquid water would reduce the weight of the fuel cell system, and thus increase the gravimetric power density. Raising the operating temperature of a PEM fuel cell would also certainly accelerate the electrode kinetics and make the replacement of expensive Pt catalysts with cheap metallic perovskite-type oxides and metal hydrides feasible. Although some alternative polymer-based protonic electrolytes have been developed such as phosphoric acid doped polybenzimidazole (PBI), their proton conductivities are either not high enough or poor for long-term stability [1–4]. Therefore, development of inorganic proton conductors and their membranes operating above 100 °C are crucial. The development of liquid-water free PEM fuel cells operating between 100 and 300 °C is a realistic and outstanding technological target. Therefore, the preparation of materials as a substitute for Nafion is now being realized.

Many attempts have been made to develop alternative materials, including oxo-acids and their salts such as sulfates, selenates, phosphates, and arsenates; organic/inorganic hybrid systems; and ceramic proton conductors such as oxides, hydroxides, and apatites [5–21]. Haile et al. [5], have claimed that $MHSO_4$

* Corresponding author. Tel.: +1 604 221 3111; fax: +1 604 221 3088.

0378-7753/$ – see front matter © 2006 Elsevier B.V. All rights reserved.
doi:10.1016/j.jpowsour.2006.03.070

presented a conduction mechanism that was independent of water content. Sulfates usually go through an order–disorder transformation followed by a significant change in electrical conductivity. However, such salts melt above 200 °C and a recent study suggested the instability of these salts in fuel cell environments [6]. Honma et al. and Li et al. have suggested some metal hydrous oxides with a high proton conductivity such as $ZrO_2 \cdot nH_2O$ and $WO_3 \cdot nH_2O$ in the intermediate temperature range of 100–300 °C [7,8]. Hybrid materials with an organic porous network filled with different inorganic proton conductive materials have been reported, including heteropolyacids [9–11], layered materials [12], and oxide particles [13–15]. Some oxygen-deficient cubic perovskites also have been studied as promising proton conductors at temperatures below 300 °C [16–18]. Several interesting reviews on the development of proton-conducting materials for technological applications have been published [19–21].

In this work, we have studied Ce-doped $Ba_2In_2O_5$ as a candidate for proton conductors for low temperatures. The oxygen-deficient perovskite materials $Ba_2In_{2-x}(M^{4+})_xO_{5-\delta}$ (M = Ce) have been produced through the Reactive Spray Deposition Technology (RSDT). The physical, chemical, and electrochemical properties of the $Ba_2In_{2-x}(M^{4+})_xO_{5-\delta}$ (M = Ce) were characterized using XRD, BET, particle size analysis, SEM, TEM, TGA/DSC/TMA thermal analysis techniques, and ac impedance spectroscopy.

2. Experimental

The oxygen-deficient perovskite materials $Ba_2In_{1.26}Ce_{0.51}O_{4.91}$ (BIC) have been produced through the RSDT. Detailed production and characterization are reported separately [22]. The solutions of Ba-, In-, and Ce-precursors were prepared according to appropriate molar ratios. During the RSDT the solution is atomized to form submicron droplets by using an atomization process. These droplets are then carried by convection in an oxygen stream to a reactor. The synthesized particles are then collected through a bag-filter. The heat from the reactor provides the energy required to evaporate the droplets and for the precursors to react to form the desired phase. The powders were then pressed into pellets under 150 MPa pressure and sintered at 1250 °C for 6 h to obtain samples for conductivity measurements. The ac impedance was performed using an impedance analyser IM6 by Zahner Electroniks with a frequency between 8 MHz to 100 mHz and at temperatures from 100 to 250 °C. The electrical conductivities were assessed in different atmospheres including nitrogen and a mixture of hydrogen and nitrogen at different ratios. Flow rates were set to 100 sccm for each atmosphere. A layer of Au was sputtered onto the sintered sample as contact electrodes. The temperature and gas flow rate were programmed using an AMI test station. Humidity was generated and controlled by a SETARAM WETSYS system. Gas lines were heated to prevent condensation. Impedance data were recorded every 30 min using the Zahner IM6 electrochemical test system. To reach equilibrium the sample was held for 2 h at each atmosphere and the impedance measurement was recorded every 30 min.

Powder samples of as-synthesized and calcined $Ba_2In_2O_5$ doped with ceria (BIC) were analyzed at room temperature by X-ray diffraction (XRD) using a Bruker AXS D8 X-ray diffractometer with a Cu Kα source in order to determine the phases. The microstructures of the sintered samples were examined using a Hitachi S-3500N scanning electron microscope (SEM). The thermal properties of the powder materials were evaluated using SETARAM Setsys Evolution thermal analysis instrument under different atmospheres.

3. Results and discussion

3.1. Effect of humidity on the electrical conductivity

The electrical conductivity of BIC was measured as a function of humidity at different temperatures in order to study the effect of humidity on conductivity and to understand the conduction mechanism in BIC. Pt and Ag paste have been employed as contact electrodes, however, reactions were observed between the BIC sample and the electrodes for both the Pt and Ag paste. Au was sputtered onto the sintered BIC disc and was found inert to the BIC sample during the electrical conductivity measurement. The BIC disc sintered at 1250 °C for 6 h had a typical diameter of 16 mm and thickness of 0.7 mm. The electrode areas were typically of 0.316 cm^2. The relative density of sintered BIC was about 92.5%, determined by Achimede method with calibration. The microstructure of the sintered BIC was examined using a SEM. The existences of micropores are observed from the SEM image as shown in Fig. 1.

The electrical conductivities of BIC were measured in an atmosphere of 50% H_2 balanced with N_2 under conditions with and without the existence of water at different temperatures, respectively. The plots of electrical conductivities of BIC are depicted in Fig. 2. It is shown that the electrical conductivities of BIC are independent to the change in atmosphere. Since the water content is only 3% in volume, measurements showing the effect of a high water content were carried out in the same temperature range. Again, the electrical conductivities at different temperatures are constant as a function of water content from

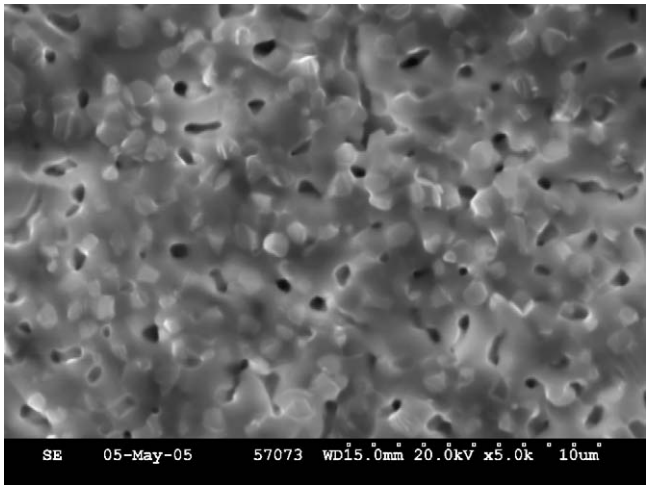

Fig. 1. Cross-section SEM image of BIC pellet sintered at 1250 °C.

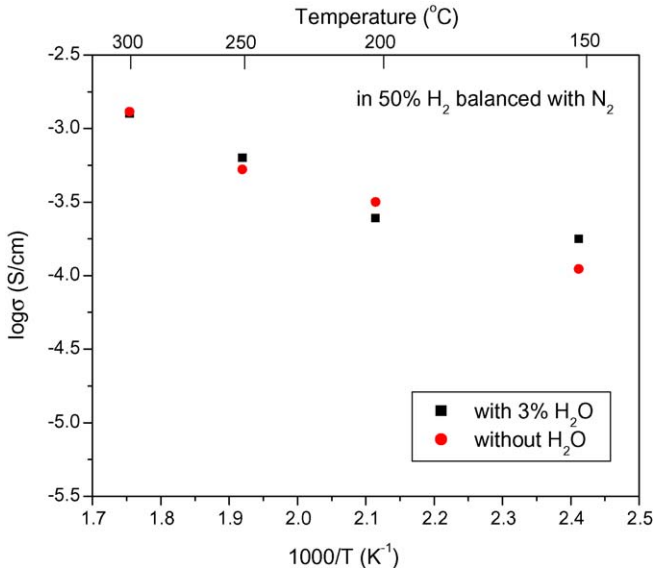

Fig. 2. Electrical conductivity of BIC as a function of temperature at different atmospheres.

10 to 30 vol% as shown in Fig. 3. Fig. 4 shows the excellent repeatability of the ac impedance under the same conditions of temperature and humidity during the measurement.

In the absence of hydrogen, the effect of moisture on the electrical conductivity was also studied. The ac impedance change of the BIC samples was recorded in an atmosphere of nitrogen with and without the 3 vol% water content. The complex impedance spectrum consists of a high frequency arc that is partially overlaid by a second arc at low frequency as shown in Fig. 5(a). In both dry and wet conditions the high frequency arcs did not go through the origin, which was most likely due to the stray impedance contribution as observed for other samples. This stray impedance could be avoided when using the water media. A calibration of the semi-circle shifting was applied for the conductivity calculation in this study. The electrical con-

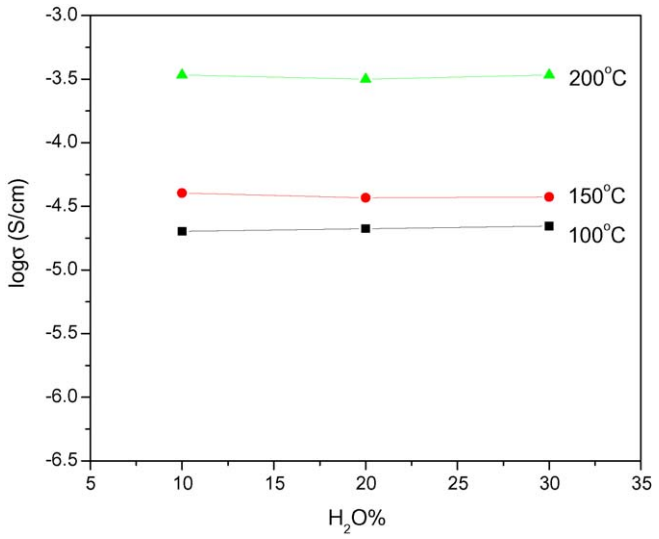

Fig. 3. Verification of electrical conductivities of BIC with water content at different temperatures.

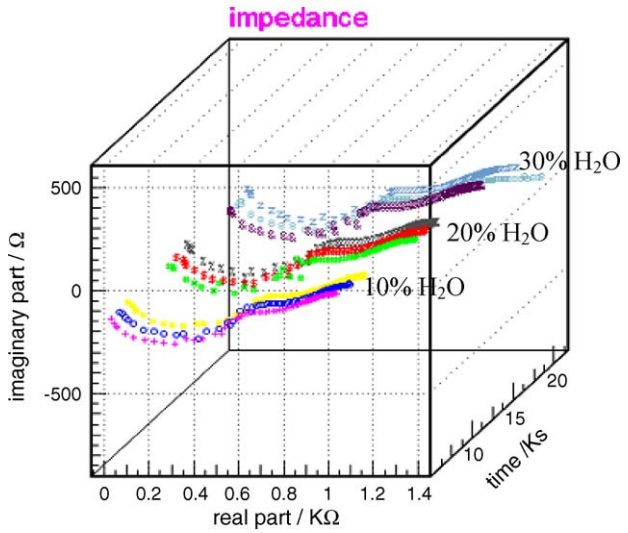

Fig. 4. Repeatability of the electrical conductivities of BIC with different humidity at 200 °C.

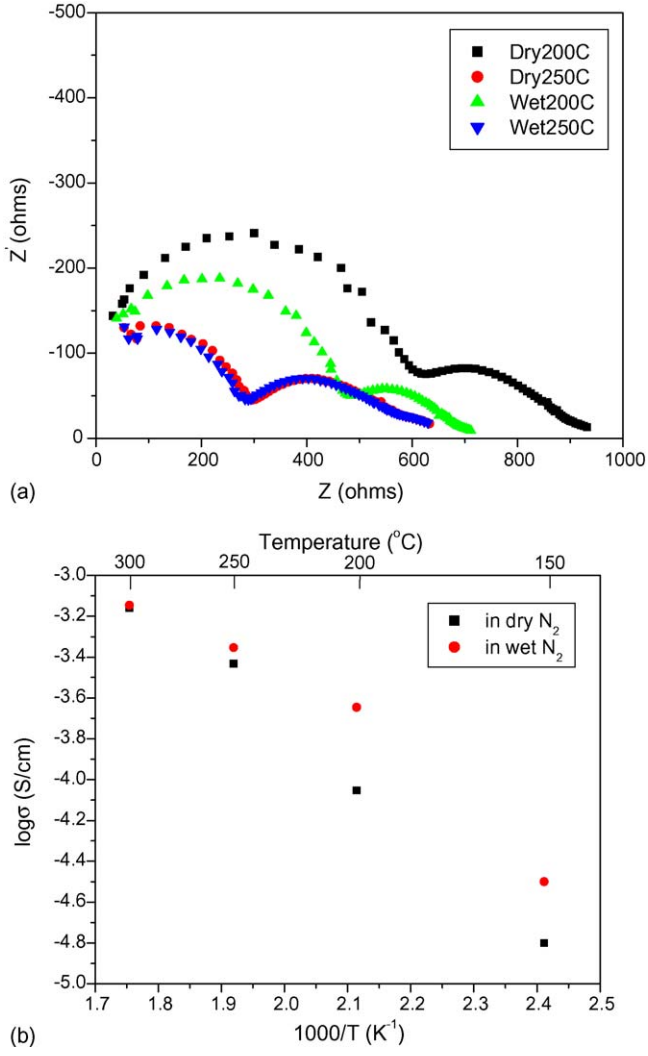

Fig. 5. (a) Typical ac impedance spectra of the BIC sample at different conditions and (b) electrical conductivity of BIC as a function of temperature in wet and dry nitrogen.

ductivities are plotted in Fig. 5(b) at different temperatures. The conductivities in wet nitrogen are greater than that in dry nitrogen in the temperature range of 150–250 °C. The effect of moisture on conductivity is less when the temperature is increased, and the conductivities are almost equal at 250 °C, which is most likely due to desorption of the adsorbed water in the BIC ceramic. The water adsorption and desorption at temperatures below 300 °C was confirmed by studying the thermal mechanical behavior of sintered BIC. A BIC bar-sample was pre-sintered at 1250 °C and was made free-standing for thermal mechanical analysis (TMA). The variation of the sample dimension was recorded during heating and cooling in air as shown in Fig. 6. A bending was observed during the heating process but not on the cooling one. The absorbed water in the BIC sample before the heating was removed at about 265 °C during the heating process and resulted in a bending point shown in Fig. 6. However, no bending point occurred when the sample was cooled down from a high temperature without water absorption. Feng and Goodenough have demonstrated similar results relating considerable water absorption occurring in undoped $Ba_2In_2O_5$ just below 300 °C [23]. On the other hand, the water content in the BIC may also lead to the change in structure and therefore the chance of thermal expansion behavior. Several groups have previously reported that H_2O in the gas phase easily interacts with $Ba_2In_2O_5$-based materials and form appropriate structure [24–27]. Hashimoto et al. claimed a reversible structural transformation between orthorhombic and tetragonal on absorption and secession of H_2O [25]. Fischer et al. proposed that the ordered oxygen vacancies within the tetragonal In–O layer in $Ba_2In_2O_5$ were accessible for H_2O molecules and that the crystal structure changed with the introduction of H_2O at the oxygen vacancies [27].

The observed different phenomena of the effect of water on the electrical conductivity of BIC can be understood by the following discussion. The proton content increases with the concentration of oxygen vacancies ($V_O^{\bullet\bullet}$) in these compounds since $Ba_2In_2O_5$-based materials are mixed oxygen and proton conductors [28,29]. Stotz and Wagner [30] suggested the following mechanism of proton incorporation:

$$(H_2O)gas + V_o^{\bullet\bullet} + O_o \rightarrow 2OH_o^{+} \quad (1)$$

The water molecule is dissociated at the surface during the incorporation reaction. The oxygen atom fills an O-vacancy close to the surface and the two protons become associated with two O-atoms, forming protonic defects with a positive effective charge. The introduction of protons into the perovskite ceramic generally is shown in terms of moisture containing gas streams as an acid/base equilibrium between water molecules and oxygen vacancies. Using Kröger-Vink notation, oxygen vacancies, $V_o^{\bullet\bullet}$, react with water to fill lattice positions with oxide ions, O_o, and produce interstitial protons, H_i^{+}, according to,

$$H_2O + V_o^{\bullet\bullet} \rightarrow O_o + 2H_i^{+} \quad (2)$$

However, due to the small size of protons, the protons do not occupy a true interstitial site but attach to oxide ions, thus forming a hydroxyl ion OH_o^{+} [31–33],

$$O_o + H_i^{+} \rightarrow OH_o^{+} \quad (3)$$

so that the net reaction demonstrating the interaction of oxygen vacancies with water vapor producing proton charge carriers can be written as,

$$H_2O + V_o^{\bullet\bullet} + O_o \rightarrow 2OH_o^{+} \quad (4)$$

However, when hydrogen is present, the hydrogen can be incorporated into the BIC directly and play a more important role than that of moisture. The hydrogen in the gas stream is incorporated directly into the material as protons and electrons (e') through an interaction with oxide ions according to,

$$\tfrac{1}{2}H_2 + O_o \rightarrow OH_o^{+} + e' \quad (5)$$

The conditions or processes occurring at opposite surfaces of the membrane drive conduction of proton and electrons across the ceramic membrane. Comparing the effect of moisture and hydrogen on the electrical conductivities measured in this study, the reaction (5) is the predominant one rather than that of reaction (2), even though the BIC is hydrophilic.

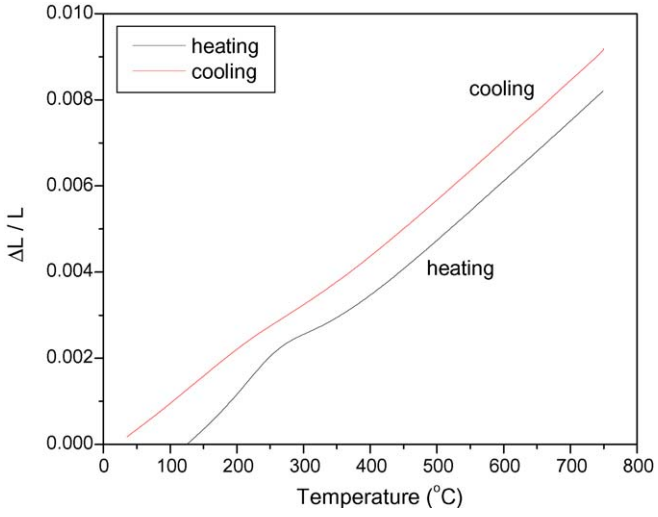

Fig. 6. The thermal mechanical behavior of sintered BIC bar-sample during heating and cooling.

3.2. *Effect of H_2 concentration on the electrical conductivity*

The effect of hydrogen concentration on the electrical conductivity of BIC was studied. When the atmosphere was changed from dry N_2 to 50% H_2, the electrical conductivity increased significantly at 100 °C as shown in Fig. 7. The electrical conductivities are relatively constant with hydrogen concentration. This suggests the presence of protonic conductivity in the BIC. Similar results were observed at elevated temperatures and Fig. 8 summarizes the results for two BIC samples at 250 °C.

The charged oxygen vacancies and the protonic ions are the main two charge carriers in the BIC materials. Since the size of oxygen vacancies is much larger than that of protonic ions, the mobilities of oxygen vacancies are much smaller than that of protonic ions, particularly at the low temperature range from

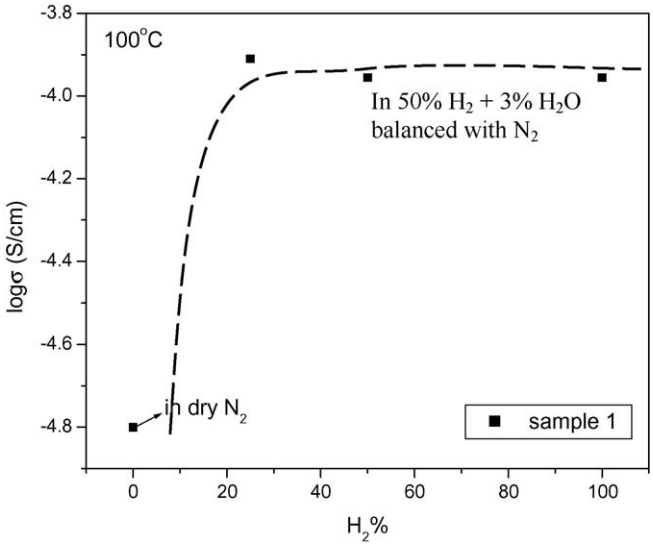

Fig. 7. Effect of hydrogen concentration on the conductivity of BIC at 100 °C.

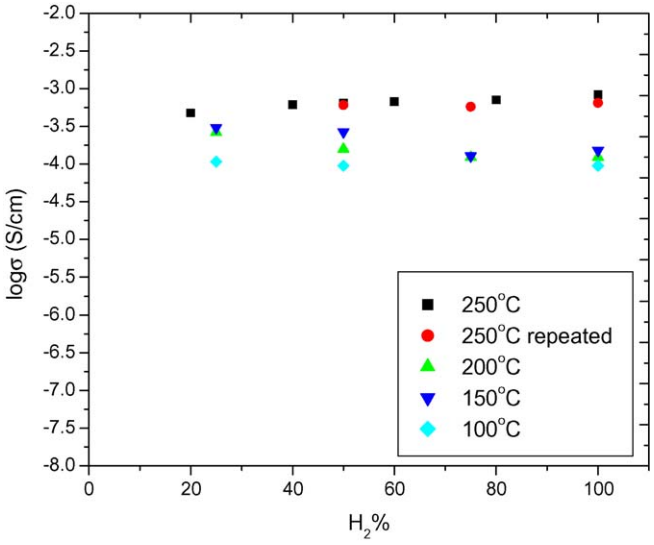

Fig. 9. Protonic conductivity of BIC at different temperatures.

150 to 250 °C [31–33]. Therefore, the contribution of charged oxygen vacancies to the total electrical conductivity should be negligible in this situation. Assuming other charge carriers do not influence the total conductivity, the protonic conductivity in BIC can be estimated from the total conductivity from the difference between the conductivity in dry N_2 and in hydrogen:

$$\sigma_H = \sigma_{H_2} - \sigma_{N_2} \quad (6)$$

In such a way, the protonic conductivities of BIC at temperatures from 100 to 250 °C are plotted in Fig. 9. The protonic transference number of the protonic conductivity is summarized in Table 1. Electronic conduction is expected because equal amounts of protons and electrons are generated according to reaction (5). Moreover, the protonic transference number would decrease when the temperature increases since ions are known to have a lower mobility than electrons. However, the decrease in the protonic transference number of BIC might also result from the existence of oxygen ionic conduction when the temperature is increased.

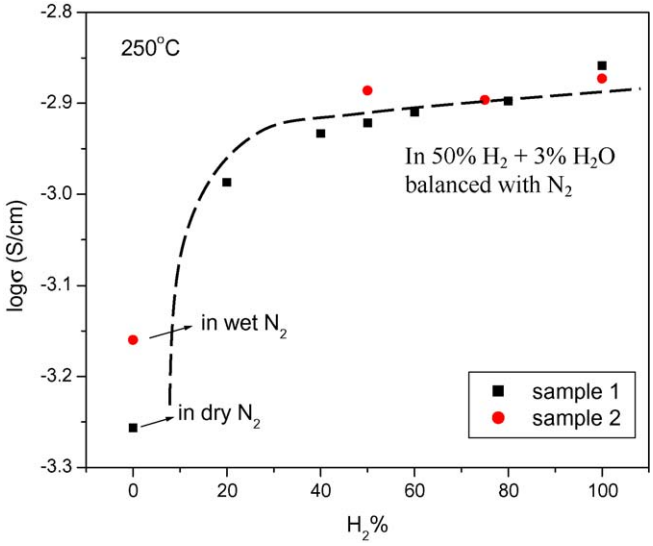

Fig. 8. Effect of hydrogen concentration on the conductivity of BIC at 250 °C.

The open circuit voltage (OCV) was measured at 280 °C using the BIC as electrolyte materials in order to further confirm the existence of the ionic conduction. The leak rate of the sintered BIC pellets was measured by pressurizing one side of the sample sintered at 1250 °C with 1 psig of helium and measuring the gas flow at the other side using a micro-flow meter. A flow rate of 0.036 sccm was observed after stabilization of the He flow after 15 min. The pellets were then coated on both sides with platinum paste and dried at 100 °C for 1 h. The cells were bonded to an alumina tube using Ceramabond® 552 to ensure gas tightness. The anode side was purged with nitrogen before introducing hydrogen. An OCV value of 0.87 V was attained and was relatively stable during the running period of 60 h for a BIC pellet at 280 °C with hydrogen as a fuel as shown in Fig. 10. However, this OCV value was still lower than the theoretical value of 1.12 V calculated from Nernst equation at 280 °C, assuming only proton conduction. There were few reasons that might cause the low OCV such as the density of the pellet and the possible electronic conduction in the materials. As summarized in Table 1, the protonic transference number of BIC was smaller than one, suggesting the existence of the electronic conduction. This table also shows that the protonic transference number increased when the temperatures decreased. It is supposed that electronic conduction was most likely the main reason for the low OCV value. In our case, the hydrogen crossover through the BIC electrolyte was also possible since the BIC sample sintered at 1250 °C only had a relative density of 92.5%. The porosity in the sintered

Table 1
Protonic transference number of BIC at different temperatures

	Temperature (°C)			
	100	150	200	250
Transference number	0.86	0.81	0.52	0.47

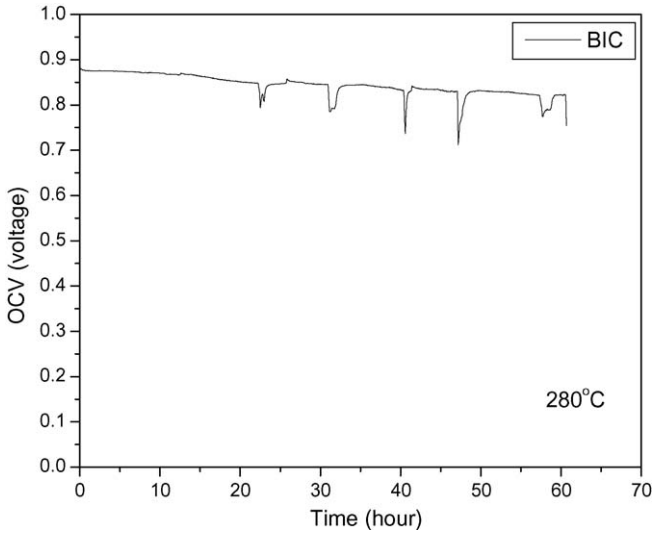

Fig. 10. Open circuit voltage of sintered BIC at 280 °C.

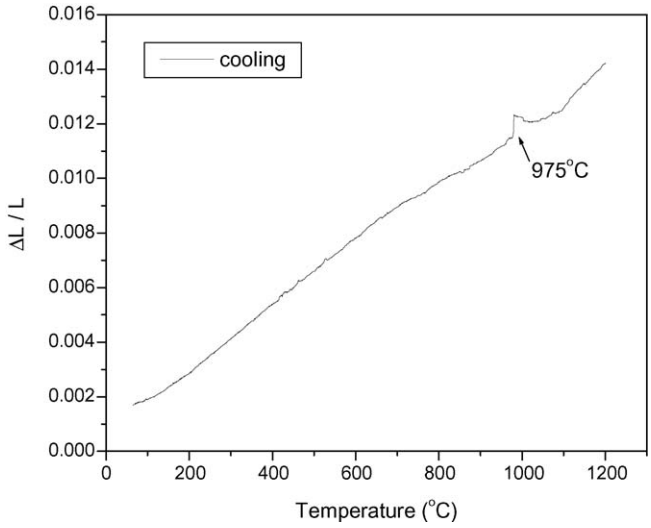

Fig. 12. Thermal expansion of sintered BIC as a function of temperature.

BIC might also result in the OCV degradation from 0.87 to 0.85 V during 60 h. It was not clear what might have caused the spike-like drops in the OCV during the long-term testing. One possibility was the hydrogen flow rate might not be constant with the flow meter. Therefore, a variation of oxygen partial pressure was expected, which might lead to the floating of the OCV.

The long-term stability of the electrolyte is a practical concern in terms of chemical stability and electrical stability. The electrical conductivity of BIC was measured during a period of 1 month. The conductivity was recorded under the same conditions such as atmosphere and temperature. Although the sample had experienced different conditions during this period, repeatable electrical conductivity was obtained and is shown in Fig. 11.

3.3. Thermal properties

In order to understand the thermal properties of BIC for electrode/electrolyte fabrication as a next stage, the coefficient of thermal expansion of BIC was studied. A free standing rectangular bar of BIC was used to conduct the thermal expansion coefficient measurement. The BIC powders were shaped by pressing and then sintering at 1250 °C for 6 h. The final rectangular bar had a size of 9.8 mm × 4.0 mm × 0.8 mm. The thermal expansion of the BIC sample was measured in air as a function of temperature with a heating rate of 3 °C min^{-1} using the SETARAM Setsys Evolution thermal analysis instrument. The thermal expansion behavior of the BIC is shown in Fig. 12. A bending thermal expansion was observed at about 975 °C, which was reported for $Ba_2In_2O_5$-based materials at 800–1000 °C depending on compositions [34–36]. The coefficient of thermal expansion of BIC is 11.2×10^{-6} K^{-1} from 25 to 1250 °C. The bending normally corresponds to a phase or oxygen vacancy order–disorder transition in the $Ba_2In_2O_5$ system. Corresponding to the phase transition from ordered oxygen vacancy to disordered in $Ba_2In_2O_5$ at 920 °C, the oxygen ionic conductivity also significantly increased as reported by Zhang and Smyth [28]. Mitamura, et al., have claimed that doping large cation at the In-site, such as La^{3+} and Y^{3+}, could reduce the transition temperature [36].

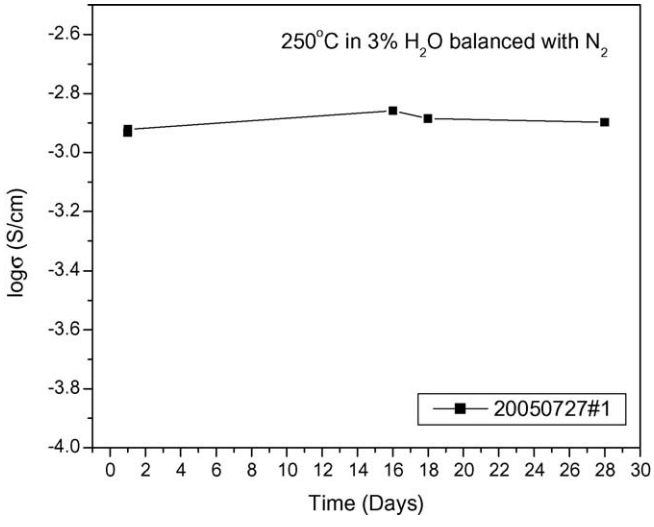

Fig. 11. Long-term stability of electrical conductivity of BIC at 250 °C.

4. Conclusions

A study of electrical and thermal properties of sintered pellets from the nanopowders was performed. The electrical conductivities were measured using ac impedance spectroscopy under different atmospheres and temperatures. The electrical conductivity of sintered BIC was found sensitive to the environmental humidity when the temperature was below 300 °C, indicating that water is being incorporated into the materials and is contributing to electrical conduction. However, in the presence of hydrogen, the electrical conductivities were independent of water content in the range of 0–30 vol%. In this case, the protons were directly incorporated into the lattice from hydrogen, which dominated the electrical conductivities. The electrical conductivities of BIC were significantly affected by the presence of hydrogen in the temperature range

of 100–300 °C, suggesting the existence of proton conduction in the BIC materials. The electrical conductivity was as high as 7×10^{-3} S cm^{-1} at 300 °C in an atmosphere of 50% hydrogen and balanced with nitrogen. The long-term stability of the electrical conductivity was performed under the same conditions. Stable conductivities were achieved for a period of 28 days at 250 °C. The activation energy E_a of 16.5 kJ mol^{-1} was obtained for BIC from a least-squares fit to an Arrhenius plot of the conductivities.

The proton transference numbers were estimated to be around 0.86 at 100 °C by comparing the conductivities in the atmospheres with and without hydrogen. An OCV value of 0.87 V was attained for a BIC pellet for a period of 60 h at 280 °C with hydrogen as a fuel. This study revealed that the BIC was a mixed electronic and ionic conductor. As summarized in Table 1, the protonic transference number of BIC increased when the temperatures decreased. Therefore, BIC is not appropriate as an electrolyte material, but can be a promising candidate as electrode materials.

The comparison of the electrical conductivities for BIC sintered at different temperatures indicates the effect of crystal structure on electrical conductivities. Low temperature sintering to maintain the brownmillerite structure was preferred for the high conductivity, which can be done via the RSDT process for thin film fabrication. A bending of thermal expansion was observed at about 975 °C, which was consistent with the previous report. The coefficient of thermal expansion of BIC is 11.2×10^{-6} K^{-1} from 25 to 1250 °C.

Acknowledgement

The authors would like to thank the New Energy and Industrial Technology Development Organization of Japan (NEDO) for financial support.

References

[1] J. Rozière, D.J. Jones, Ann. Rev. Mater. Res. 33 (2003) 503–555.
[2] P. Staiti, M. Minutoli, J. Power Sources 94 (2001) 9–13.
[3] P. Staiti, J. New Mater. Electrochem. Syst. 4 (2001) 181–186.
[4] P. Staiti, Mater. Lett. 47 (2001) 241–246.
[5] S.M. Haile, D.A. Boysen, C.R.I. Chisholm, R.B. Merle, Nature 410 (2001) 910–913.
[6] R.B. Merle, C.R.I. Chisholm, D.A. Boysen, S.M. Haile, Energy Fuels 17 (2003) 210–215.
[7] I. Honma, Y. Takeda, J.M. Bae, Solid State Ionics 120 (1999) 255–264.
[8] Y.M. Li, T. Hibino, M. Miyayania, T. Kudo, Solid State Ionics 134 (2000) 271–279.
[9] S. Malhotra, R. Datta, J. Electrochem. Soc. 144 (1997) 123–133.
[10] B. Tazi, O. Savadogo, Electrochim. Acta 45 (2000) 4329–4339.
[11] B. Tazi, O. Savadogo, J. New Mater. Electrochem. Syst. 4 (2001) 187–196.
[12] G. Alberti, M. Casciola, Annu. Rev. Mater. Res. 33 (2003) 129–154.
[13] K.A. Mauritz, R.M. Warren, Macromolecules 22 (1989) 1730–1734.
[14] S.P. Nunes, B. Ruffmann, E. Rikowski, S. Vetter, K. Richau, J. Membr. Sci. 203 (2002) 215–225.
[15] S. Li, M. Liu, Electrochim. Acta 48 (2003) 4271–4276.
[16] J.B. Goodenough, A. Manthiram, P. Paranthaman, Y.S. Zhen, Solid State Ionics 52 (1992) 105–109.
[17] T. Norby, Y. Larrin, Curr. Opin. Solid State Mater. Sci. 2 (1997) 593–599.
[18] D. Yang, A.S. Nowick, Solid State Ionics 91 (1996) 85–91.
[19] T. Norby, Solid State Ionics 125 (1999) 1–11.
[20] K.D. Kreuer, Chem. Mater. 8 (1996) 610–641.
[21] K.D. Kreuer, Solid State Ionics 97 (1997) 1–15.
[22] R. Maric, C. Decès-Petit, R. Hui, X. Zhang, D. Ghosh, K. Sakata, M. Kenji, J. Electrochem. Soc., in press.
[23] M. Feng, J.B. Goodenough, MRS Symp. Proc., vol. 369, Materials Research Society, 1995, pp. 333–342.
[24] T. Schober, J. Friedrich, F. Krug, Solid State Ionics 99 (1997) 9–13.
[25] T. Hashimoto, Y. Inagaki, A. Kishi, M. Dokiya, Solid State Ionics 128 (2000) 227–231.
[26] T. Schober, J. Friedrich, Solid State Ionics 113–115 (1998) 369–375.
[27] W. Fischer, G. Reck, T. Schober, Solid State Ionics 116 (1999) 211–215.
[28] G.B. Zhang, D.M. Smyth, Solid State Ionics 82 (1995) 153–160.
[29] J.B. Goodenough, J.E. Ruiz-Diaz, Y.S. Zhen, Solid State Ionics 44 (1990) 21–31.
[30] S. Stotz, C. Wagner, Ber. Bunsenges. Phys. Chem. 70 (1966) 781–788.
[31] N. Bonanos, B. Ellis, K.S. Knight, M.N. Mahmood, Solid State Ionics 35 (1989) 179–188.
[32] R.L. Cook, A.F. Sammells, Solid State Ionics 45 (1991) 311–321.
[33] A.F. Sammells, R.L. Cook, J.H. White, J.J. Osborne, R.C. MacDuff, Solid State Ionics 52 (1992) 111–123.
[34] H. Yamamura, Y. Yamada, T. Mori, T. Atake, Solid State Ionics 108 (1998) 377–381.
[35] M. Yoshinaga, M. Yamaguchi, T. Furuya, S. Wang, T. Hashimoto, Solid State Ionics 169 (2004) 9–13.
[36] T. Mitamura, H. Ogino, H. Kobayashi, T. Mori, H. Yamamura, J. Am. Ceram. Soc. 76 (8) (1993) 2127–2128.